Unconventional Terahertz Carrier Relaxation in Graphene Oxide: Observation of Enhanced Auger Recombination Due to Defect Saturation

Jaeseok Kim,[†] Juyeong Oh,[‡] Chihun In,[†] Yun-Shik Lee,[§] Theodore B. Norris,[⊥] Seong Chan Jun,[‡,*] and Hyunyong Choi[†,*]

[†]School of Electrical and Electronic Engineering, Yonsei University, Seoul 120-749, Korea, [‡]Department of Mechanical Engineering, Yonsei University, Seoul 120-749, Korea, [§]Department of Physics, Oregon State University, Corvallis, Oregon 97331-6507, United States, and [⊥]Center for Ultrafast Optical Science and Department of Electrical Engineering and Computer Science, University of Michigan, Ann Arbor, Michigan 48109, United States

ABSTRACT Photoexcited carrier relaxation is a recurring topic in understanding the transient conductivity dynamics of graphene-based devices. For atomically thin graphene oxide (GO), a simple free-carrier Drude response is expected to govern the terahertz (THz) conductivity dynamics—same dynamics observed in conventional CVD-grown graphene. However, to date, no experimental testimony has been provided on the origin of photoinduced conductivity increase in GO. Here, using ultrafast THz spectroscopy, we show that the photoexcited carrier relaxation in GO exhibits a peculiar non-Drude behavior. Unlike graphene, the THz dynamics of GO show percolation behaviors: as the annealing temperature increases, transient THz conductivity rapidly increases and the associated carrier relaxation changes from mono- to biexponential decay. After saturating the recombination decay through defect trapping, a new ultrafast decay channel characterized by multiparticle Auger scattering is observed whose threshold pump fluence is found to be 50 μJ/cm^2. The increased conductivity is rapidly suppressed within 1 ps due to the Auger recombination, and non-Drude THz absorptions are subsequently emerged as a result of the defect-trapped high-frequency oscillators.

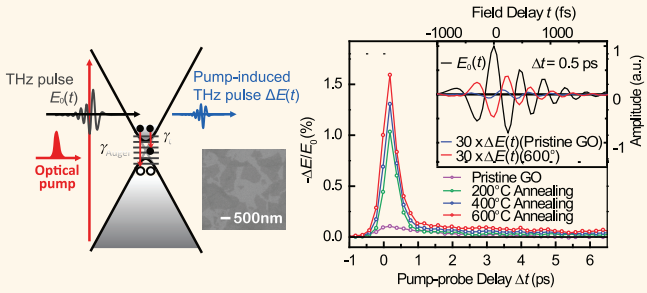

KEYWORDS: graphene · graphene oxide · Auger recombination · defect saturation · percolation behavior · ultrafast optical-pump terahertz-probe spectroscopy

Graphene, a two-dimensional (2D) carbon material with honeycomb lattice, has received tremendous attention in optoelectronic and photonic applications because of its distinct 2D electronic and optical properties.[1−4] Chemical exfoliation methods producing graphene oxide (GO) from graphite present a promising scheme to achieve solution-processable large-area graphene synthesis and related devices.[5−10] The solution-based GO, however, inevitably contains lattice defects due to oxygen-functionalized groups that destroy the Dirac-like linear dispersion.[11−15] Recent work has observed the existence of far-infrared energy gap (10−50 meV), depending on the oxygen reduction process, which leads to the insulator-semimetal transitions.[12] Thus, unlike graphene, the carrier relaxation dynamics in GO is strongly influenced by recombination kinetics associated with the defect trapping, and the relaxation pathways are expected to be different from those of graphene.

To date, most of the ultrafast studies on various graphene layers[16,17] have focused on understanding the optical and terahertz (THz) response of linear-dispersion characteristics.[18−22] Prior pump-fluence dependent studies (both theoretical and experimental investigations) have reported that the photoexcited carriers decay *via* energy

* Address correspondence to scj@yonsei.ac.kr, hychoi@yonsei.ac.kr.

Received for review November 25, 2013 and accepted February 4, 2014.

Published online February 04, 2014
10.1021/nn406066f

© 2014 American Chemical Society

dissipation arising from coupling between carriers and phonons at low pump fluence or *via* carrier−carrier scatterings resulting in Coulomb-mediated momentum redistribution of hot carriers at high pump fluence within 1 ps.[23,24] These studies of ultrafast carrier relaxation pathways have made important contributions to the development of novel graphene-based optoelectronic devices,[25−28] which were also demonstrated in other carbon materials such as carbon nanotubes[29−32] and nanoscale quantum dots.[33−35]

In GO, the defect-mediated dynamics should play a key role in governing the carrier relaxation, yet the rapid carrier-relaxation mechanisms have not been clearly identified. For example, although recent equilibrium spectroscopies in GO have clearly shown that the defect-assisted high-frequency absorption oscillators are distributed in the THz range,[11,13,36,37] analysis on the nonequilibrium carrier relaxation dynamics (hundreds of fs decay) relies on carrier−carrier and carrier-phonon scattering of intrinsic Dirac quasiparticles,[38,39] *i.e.*, the same characteristic dynamics of graphene appeared in exfoliated, epitaxial- or CVD-grown graphene. To date, no ultrafast carrier dynamics in GO has been reported in the THz frequency range, and the defect-trapping and recombination pathways have been barely understood. We note that because the physical mechanisms of free-carrier relaxation in GO are different from those of graphene, ultrafast THz studies may offer alternative ways of controlling the carrier relaxation pathways, and potentially contribute to development of efficient GO-based optoelectronic devices.

The primary aim of this paper is to investigate the role of defects on the carrier relaxation pathways in GO. We present the transient changes of THz response of various types of GO in order to identify the free-carrier relaxation pathways depending on the excited pump fluence *F*. Because of the small photon energy of the THz radiation (4.1 meV at 1 THz), THz probes can directly access the low-energy free-carrier response to the photoexcitation. The defect properties of GO were systematically altered *via* thermal annealing in order to gradually reform the defect-rich GO characteristics into the graphene-like ones. Specifically, we employ high *F* up to 100 μJ/cm^2 that excites large amount of carriers, which is strong enough to saturate the trap states in GO. We observe a new recombination pathway in annealed GO samples, which follows Auger recombination that governs the initial free-carrier decay under high *F* excitation. The extracted time constant decreases with a threshold-like behavior as *F* increases above 50 μJ/cm^2. Corresponding THz peak of transient conductivity signals are saturated as a function of one-third order of *F*. Quantitative analysis based on a simple two-level rate equation including the trap-associated dynamics and the Auger recombination strongly corroborates our experimental observations.

RESULTS AND DISCUSSION

In our study, four samples including a pristine GO and annealed GO samples of 200, 400, and 600 °C on quartz substrates are prepared to investigate the defect-density-dependent carrier relaxation dynamics. To confirm the different carbon groups in GO, we performed XPS measurements (Thermo U. K. k-alpha). Figure 1a shows C_{1s} spectrum for various GO samples as a function of binding energy. Each peak corresponds to carbon groups with sp^2 chemical structure at 284.4 eV, sp^3 at 285.4 eV, O−C−O/O−H at 286.2 eV, C═O at 287.8 eV, O−C═O at 288.5 eV, and COOH at 289.3 eV.[40,41] Since the GO mainly consists of carbon atoms with honeycomb lattice, the major peak related to the sp^2 configuration is positioned at 284.4 eV. In particular, the pristine GO sample shows large secondary peak (orange) at 285.4 eV that is correlated to the sp^3 configurations representing disorder or defect-rich characteristics; however, the relative intensity ratio of 284.4 eV (olive) to 285.4 eV (orange) increases with increasing temperature because the thermal annealing affects the restoration process of sp^2 hybridization from sp^3 hybridization. Other peaks related to oxygen-related functional groups decrease with increasing annealing temperature. Therefore, while graphene has a linear band structure with a cone shape between conduction and valence band, GO has a gap associated with defect levels resulting from the disorder or the oxygen functional groups. As shown by AFM (Park systems XE-100) images in Figure 1b, the average thickness of GO samples is around 25−28 nm (approximately 20 layers of GO flakes), and each sample appears to be uniformly deposited with the same amount. Figure 1c shows the UV−visible absorbance spectra of the GO samples (using Shimadzu UV-1800). Compared to the pristine GO sample, the annealed GO sample of 600 °C shows stronger excitonic resonance at 4.6 eV,[42] representing the characteristics of single-layer graphene and the absorbance at 800 nm is about 3 times larger than that of the pristine GO sample. We verified that the flake size of the chemically exfoliated GO is around 0.2−1 μm and the filling factor *f* of the GO flakes is about 60−70% using SEM image as shown in the inset of Figure 1c.

Ultrafast optical-pump THz-probe spectroscopy was performed using a 50 fs, 250 kHz Ti:sapphire regenerative amplifier system (Coherent RegA 9050) that excites the samples with photon energy of 1.55 eV. To measure the time-resolved THz signals, the THz pulses covering photon range of 3−11 meV are generated by optical rectification and detected by electro-optic sampling technique in a pair of 0.5 mm thick, (100)-oriented ZnTe crystal; see the Supporting Information for more details on the experimental setup. All measurements were performed at room temperature. Figure 1d shows an experimental scheme depicting the effects of defect states which severely obscure the

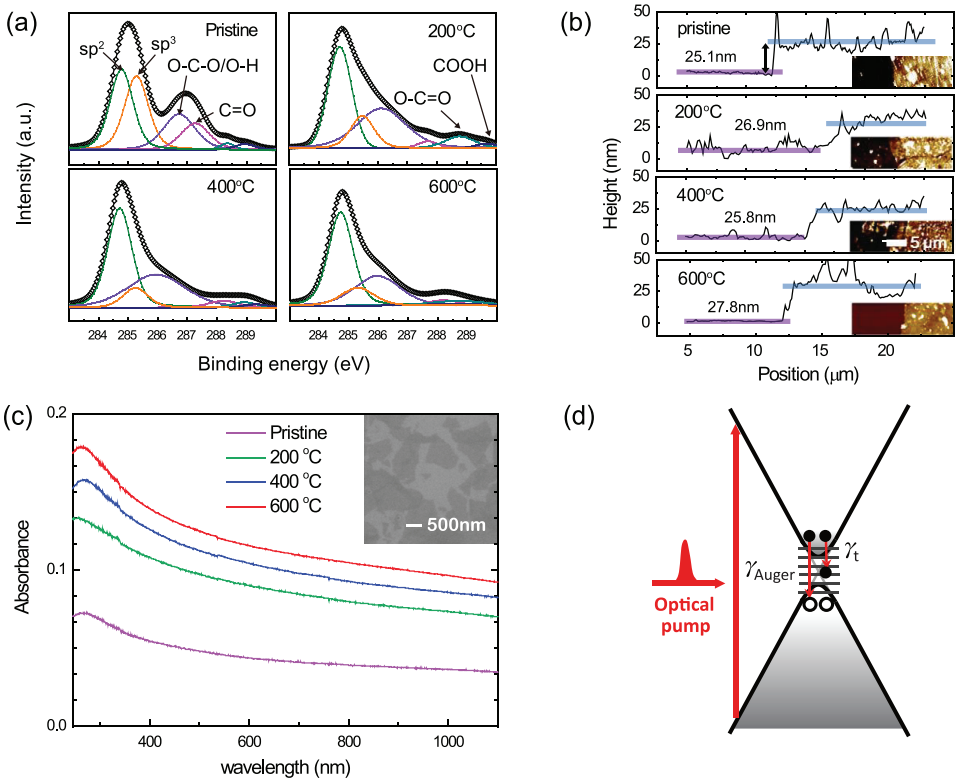

Figure 1. (a) XPS spectra of pristine and annealed GO samples. The measured data (black diamond) are fitted by simple Gaussian functions (color lines). The ratio of sp^2 at 284.4 eV to other oxygen functional groups rapidly increases when GO is annealed at temperature higher than 200 °C, indicating the property of GO undergoes an abrupt change. (b) AFM images show the height of each sample is about 25−28 nm. (c) UV−visible absorbance spectra from 240 to 1100 nm. Inset: SEM image of a monolayer GO film. On the basis of the image analysis, the estimated filling factor of GO flakes is around 0.6−0.7. (d) A decay process of photoinduced carriers in the GO samples is shown on top of the band structure. Unlike pristine graphene, GO samples contain defect states in THz range.

linear Dirac-dispersion property in the THz frequency range. In general, when an ultrashort pulse excites the GO samples across the valence to the conduction band, highly nonequilibrium carriers are rapidly thermalized to the low-energy states of conduction band within tens of femtosecond *via* optical phonon emission and carrier−carrier scattering.[18,20] The main issue is the decay dynamics of these thermalized carriers, specifically the role of defect-trapped decay rate (γ_t) and the nonradiative decay channel after saturating the defects under high pump-excitation condition. Later, we show that the Auger-scattering rate (γ_{Auger}) undergoes substantially increased behavior as the defect-mediated decay is saturated, and this effect becomes more significant as the submicrometer spatial confinement of the GO samples (the dimension is two or three order smaller than the wavelength of 300 μm at 1 THz) increases with increasing the annealing temperature.

Figure 2a shows the pump-induced changes of THz peak signals for various GO samples with different annealing temperatures as a function of the pump−probe delay Δt. As shown in the inset of Figure 2a, the opposite sign between $\Delta E(t)$ and the reference THz field $E_0(t)$ indicates pump-induced increased carrier density.[43] We note that the measured $\Delta E(t)$ of the pristine and 600 °C annealed GO samples displays significantly different amplitude and phase (see the blue and red THz traces in the inset); these field-resolved THz traces are used later to analyze the complex conductivity in the frequency domain. For the decay dynamics shown in main panel of Figure 2a, while the amplitude change of the pristine GO sample is relatively small and decays monoexponentially, the peak $\Delta E(t)$ dynamics of the annealed GO samples contains rapidly decaying components within Δt of 1 ps, and the subsequent decay exhibits slow relaxation in tens of picosecond. These abrupt changes of peak amplitude and decay dynamics seemingly appear when the annealing temperature is higher than 200 °C. In other words, the measured changes of THz conductivity reflect the percolation behavior. As discussed later on the spectral analysis (Figure 4), the DC conductivity of the pristine GO sample, *i.e.*, $\Delta\sigma_1(\omega = 0, \Delta t = 0)$, are fully suppressed, exhibiting a non-Drude response. On the other hand, the corresponding DC conductivity of the annealed GO samples is significantly increased, indicating the presence of free-carrier Drude response for the annealed GO. This increased Drude response represents the percolation behavior that is quite

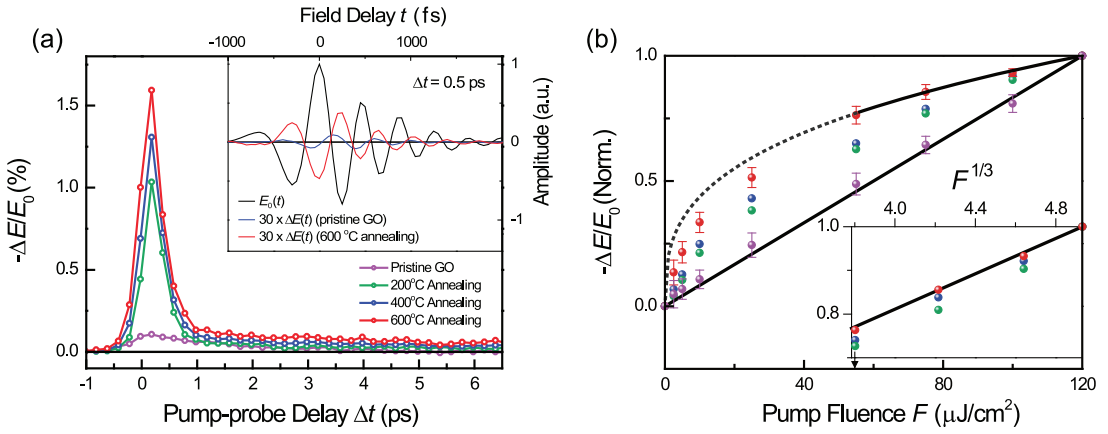

Figure 2. (a) The transient THz peak dynamics for various GO samples with different annealing temperature. Inset: THz filed traces of pristine and 600 °C annealed GO samples at $\Delta t = 0.5$. (b) Peak THz amplitude as a function of F. The measured data show a one-third order function of F when annealing temperature is increased. Inset: signals converted to one-third order dependence of pump fluence for $F > 50\ \mu J/cm^2$.

different between the pristine and annealed GO samples. Recent investigations show that this percolation action arises from the reduced number of defect states by increasing the annealing temperature.[44] Because the number of defect states is relatively small in the annealed GO samples, it is expected that the defect-mediated decay play a different role in determining the relaxation pathways between the pristine and the annealed GO samples.

To further understand the role of defects, we have performed F-dependent measurements. Figure 2b displays the normalized THz peak signals $-\Delta E(t)/E_0$ as a function of F. To exclude the saturation effect of the optical absorption (which typically occurs at F of 2 mJ/cm^2),[22] we have limited F below 100 μJ/cm^2. In case of the pristine GO sample, the signals increase linearly with increasing F (see the purple dots). This observation differs from the case of graphene, where the nonlinear dependence of the peak $-\Delta E(t)/E_0$ is attributed to the distinguished aspect of Dirac quasiparticles arising from the linear dispersion.[43,45,46] Because the energy dispersion of GO is not linear in the THz range due to the intrinsically defect-rich characteristics, a natural explanation for the experimental observation is that the rate of carrier capture in the lattice defect is linearly proportional to the photoinduced carrier density. For the annealed GO samples, on the other hand, a saturation behavior is clearly seen with a threshold F of about $F_{th} \approx 50\ \mu J/cm^2$. Below F_{th}, the peak signals of $-\Delta E(t)/E_0$ is linear due to the defect trapping, whereas the nonlinear dependence appears above F_{th}. This F-dependent relationship in $F > F_{th}$ is best fitted with one-third order power law as shown in the inset of Figure 2b (see data for the 600 °C annealed GO sample). Because the THz peak reflects the carrier density, which is thermalized *via* carrier−carrier scattering under high pump fluence, we attribute this cubic root behavior to Auger recombination mediated by three-particle Coulomb scattering. Under high pump

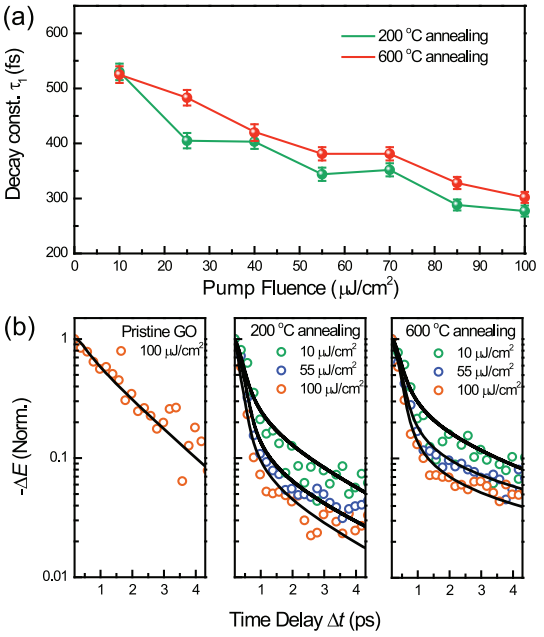

Figure 3. (a) Fast decay component of biexponential fitting from time-resolved data of Figure 2a is displayed as a function of F for 200 and 600 °C annealed GO samples. In both samples, the rapid decay with increasing F demonstrates the Auger recombination. (b) Time-resolved THz field dynamics of pristine GO, 200 and 600 °C annealed GO samples at several F. In the pristine GO sample, the defect-associated monoexponential decay is observed. In 200 and 600 °C annealed GO samples, the decay follows biexponential function with increasing F. This indicates a new decay channel *via* Auger recombination, which is significantly enhanced by the defect saturation.

excitation $F > F_{th}$, the relationship between the pump-induced THz field changes ΔE and the pump fluence F can be expressed as $-\Delta E(t = t_0)/E_0 \propto N_0 - \gamma_{Auger} N_0^3 \sim -\gamma_{Auger} N_0^3$, where t_0 is the pump−probe delay at the THz peak and N_0 is the initial carrier density just after photoexcitation.[19,20,47,48]

To investigate the dynamics of the Auger recombination pathway, we have performed time-resolved THz

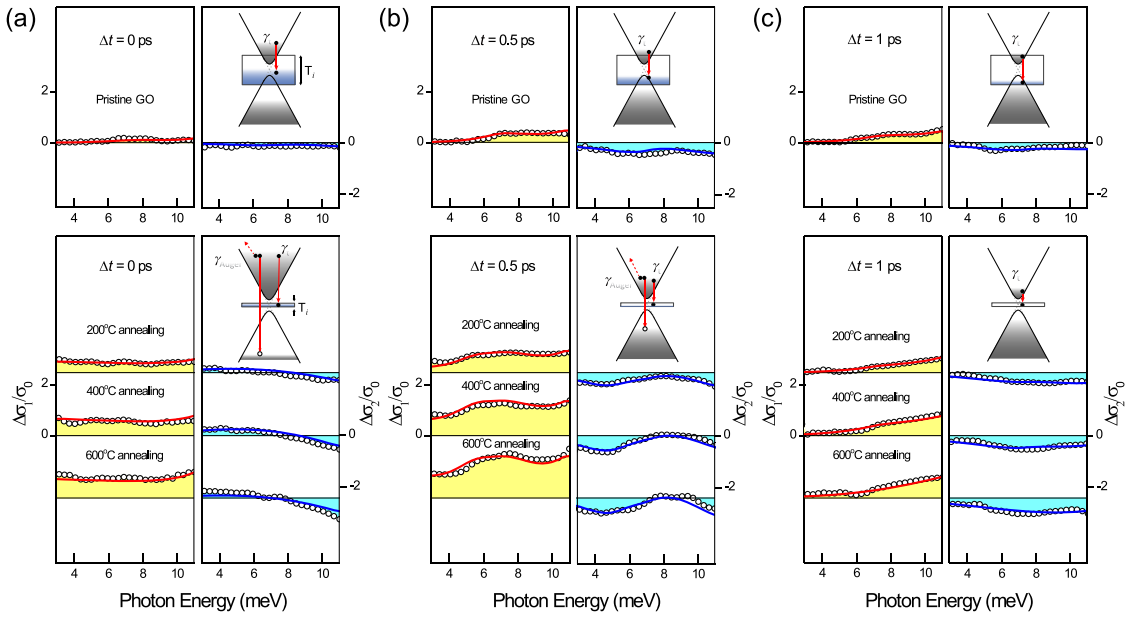

Figure 4. The pump-induced complex conductivity changes of $\Delta\sigma(\omega)/\sigma_0 = \Delta\sigma_1(\omega)/\sigma_0 + i\,\Delta\sigma_2(\omega)/\,\sigma_0$ at (a) $\Delta t = 0$ ps just after photoexcitation, (b) 0.5 ps, (c) 1 ps when F is 100 μJ/cm^2. To obtain the conductivity from the measured time-domain THz field, the data are converted to the frequency-domain using a thin-film conductivity formula of $\Delta\sigma = -1/Z_0(\Delta E/E_0)(n_S+1)$,[46] where Z_0 is the vacuum impedance, and n_S = 1.54 is the quartz substrate refractive index. Spectrally resolved THz conductivity presents defect-assisted decay in the pristine GO, and the Auger-dominant decay is enhanced by the defect saturation in the annealed GO samples.

dynamics with varying F for the pristine, 200 °C, and 600 °C annealed GO samples. Figure 3a displays the fast decay component τ_1 of biexponential function $(-\Delta E(t)/E_0 \propto dN/dt \propto A\exp(-t/\tau_1) + (1-A)\exp(-t/\tau_2))$ with increasing F for the dynamics of 200 and 600 °C annealed GO samples, respectively. As discussed later in the rate-equation analysis, that the first decay rate $(1/\tau_1)$ of the biexponential function corresponds to the fast γ_{Auger}. For the second decay rate $(1/\tau_2)$ of the biexponential function, there are two decay processes in the rate equation: one is the bulk-like relaxation of GO flakes $(1/\tau_{bulk})$ and another is the relaxation into the trap (γ_t). Between the two decay processes $(1/\tau_{bulk}$ and $\gamma_t)$, $1/\tau_{bulk}$ contributes to the constant offset with 0.05 ps^{-1} in the rate-equation model, and its rate is much smaller than the γ_t. The extracted values of τ_1 decrease with increasing F, suggesting that the Auger recombination is enhanced by the surge of the photocarrier density. As shown in Figure 3b, the time-resolved THz peak change reveals different relaxation behaviors between the pristine and the annealed GO samples. The pristine GO sample shows monoexponential decay with the decay constant of 16 ps, which is independent of F. On the other hand, the fast decay constant τ_1 of the annealed GO samples decreases with increasing F. The slow decay component shows no F dependence with the decay constant τ_2 of around 15−20 ps.

For quantitative analyses on the different dynamics with varying annealing temperatures, we have constructed a model that accounts for the charge trapping, the bulk-like GO relaxation (GO flakes without defects)[38,39] and Auger recombination pathway. When we construct the rate-equation model, we neglect the carrier-relaxation rate from the defects to the valence band.[47,49,50] This is because the defect-trapping rate is higher than that of the carrier relaxation from the defects to the valence band. Our analyses are based on the following coupled rate equations:[47,51]

$$\frac{dN(t)}{dt} = -\frac{N(t)}{\tau_{bulk}} - \gamma_t N(t)T(t) - \gamma_{Auger}(N(t))^3 + G(t)$$
$$\frac{dT(t)}{dt} = -\gamma_t N(t)T(t) \quad (1)$$

where N is the photoinduced carrier density and T is the density of unoccupied trap states. The fits (solid lines in Figure 3b) show good agreement with the time-resolved data. In the coupled rate equations, pump-induced population density $G(t)$ is the Gaussian pulse of cross-correlation between the pump and probe pulses. $G(0)$ at pump−probe delay $\Delta t = 0$ is determined by the absorbed photon density α that is given by the excited F and the graphene optical absorption $2Z_0\sigma_0/(n_S+1) \sim 1.8\%$, where Z_0 is the vacuum impedance, $\sigma_0 = e^2\pi/4h$ is the quantum conductivity, and n_S = 1.54 is the refractive index of the quartz substrate at the wavelength of 800 nm. When F is 100 μJ/cm^2, we assume that the annealed GO sample at 600 °C is excited with $\alpha = 1.2\times 10^{12}$ cm^{-2}, and the absorbed photon density of other samples are scaled with the reduced absorption at 800 nm as shown in the UV−visible spectrum of Figure 1c. The bulk recombination pathway of GO is described by a term of τ_{bulk}, which is

TABLE 1. Fitting Parameters of eq 2 Shown in Figure 4a−c

samples[a]	pristine GO			200 °C annealing			400 °C annealing			600 °C annealing		
Δt	0 ps	0.5 ps	1 ps	0 ps	0.5 ps	1 ps	0 ps	0.5 ps	1 ps	0 ps	0.5 ps	1 ps
$\omega_p/2\pi$	0	0	0	65	30	5	78	48	10	85	52	12
$\omega_{L,1}/2\pi$	18.4	0	0	0	31.8	0	0	42.1	0	0	44.7	0
$\omega_{L,2}/2\pi$	16.6	26.6	19.5	0	35.6	19.9	0	45	21	0	49.3	23
$\omega_{L,3}/2\pi$	0	74.7	71.2	50.3	79.6	75.2	67.5	100.7	87.2	70.8	118.1	95.4

[a] Units of $\omega_p/2\pi$, $\omega_{L,1}/2\pi$, $\omega_{L,2}/2\pi$, and $\omega_{L,3}/2\pi$: THz.

fitted to 20 ps. The trapping of pump-induced carrier is expressed with a coupling constant γ_t which is extracted to be 2×10^{-16}, 1×10^{-16}, 0.7×10^{-16} $cm^2\ s^{-1}$ for the pristine, 200 and 600 °C annealed GO samples, respectively. The initial free trap density T_i is extracted to be the values of 4×10^{11}, 1.2×10^{11}, and 0.8×10^{11} cm^{-2} for the pristine, 200 and 600 °C annealed GO samples, respectively. The extracted parameters corroborate the nature of defect-trapping relaxation pathway; the defect density decreases with increasing annealing temperature and the decay through defect trapping is dominant at all pump−probe delay for the pristine GO sample. For the annealed GO samples, the initial rapid decays are interpreted as an Auger recombination term with Auger coefficient γ_{Auger} of 2×10^{-21} cm^4s^{-1} for 200 and 600 °C annealed GO samples. Note that the Auger coefficient in the pristine GO (1×10^{-24} cm^4s^{-1}) is three order smaller than that of the annealed GO samples. This supports our interpretation that the dominant relaxation pathway in the annealed GO samples is the Auger recombination.

The enhanced Auger recombination pathway is further evidenced in the spectrally resolved THz response. Figure 4 shows photoexcited complex sheet conductivity changes $\Delta\sigma(\omega)$ [= σ (with pump) - σ (without pump)] at several Δt when F = 100 μJ/cm^2; the top panel is for the pristine GO and the bottom panels are for the annealed GO samples, respectively. Strictly speaking, the measured data represent the conductivity dynamics of the GO-air composite. To extract the conductivity of GO flakes, we have used the Bruggman effective medium approximation (EMA);[52] see the Supporting Information for more details. The main point of the EMA results is that we can simply rescale the conductivity of GO without significantly changing the original response of the GO-air composite. For a quantitative analysis, the experimentally obtained THz response is fitted *via* a sum of Drude and multi-oscillator Lorentz model, *i.e.*, $\Delta\sigma = \sigma_{Drude} + \sigma_{Lorentz}$:

$$\sigma_{Drude}(\omega) = \frac{i\varepsilon_0{\omega_p}^2\omega}{\omega^2 + i\omega\Gamma}$$
$$\sigma_{Lorentz}(\omega) = \sum_k \frac{i\varepsilon_0{\omega_{L,k}}^2\omega}{\omega^2 - {\omega_{0,k}}^2 + i\omega\Gamma} \quad (2)$$

where ε_0 is the free-space permittivity, Γ is the momentum scattering rate, ω_p is the plasma frequency, $\omega_{L,\ k}$ is the strength of k^{th} oscillator, and $\omega_{0,k}$ is the frequency of k^{th} oscillator. Of course, due to the nano- and microstructures of GO flakes, there is a possibility of backscattering contribution to the non-Drude response so that a Drude-Smith model might be necessary to interpret the Figure 4. However, recent investigation[53] suggests that the contribution of backscattering is not significant if f is larger than 25% or so. Given that f in our GO samples is 60−70%, we assume that the THz response can be determined by the free-carrier Drude response of GO flakes. The time-resolved dynamics between the pristine and the annealed GO provide additional evidence of the weak backscattering; if the backscattering is significant such that the DC conductivity is completely suppressed, similar phenomena should be observed both for the pristine and annealed GO samples. Figure 4 shows that the high-frequency absorption is observed for the pristine GO at Δt = 0 ps, while the corresponding spectra of annealed GO samples are rapidly varying as a function of Δt. The results of fits are shown in Figure 4 as solid lines, and the parameters are presented in Table 1. We obtain best fits with three oscillators that are resonant at 1.38, 1.85, and 3.4 THz with $\Gamma_{Lorentz}/2\pi$ of 0.8−1.6 THz in addition to the Drude-like response with $\Gamma_{Drude}/2\pi$ of 1.6−2.4 THz. The multiple oscillators are necessary to include the existence of both the distributed defect states and the small THz energy gap;[12,36,44] the effects of the two mechanisms are not distinguishable from the THz measurements.

Unlike previously reported THz dynamics of graphene, where pure Drude responses are typically observed,[19,43,46] our GO samples shows significantly different aspects. In the pristine GO sample, Figure 4a−c (top panel) shows that the DC conductivity is strongly suppressed and the defect-associated absorption oscillators overwhelm the high-frequency response for all Δt.[36,44] Whereas the multiple oscillators indicate the presence of defect states, the suppressed DC conductivity (absence of plasma frequency ω_p in Table 1) suggests that the relaxation dynamics is dominated by the single decay channel mediated by defect capture regardless of Δt. The observed monoexponential decay of time-resolved dynamics in Figure 3b supports this scenario with negligible contribution of the Auger recombination channel to the decay dynamics. For the annealed GO samples (bottom panels in Figure 4a−c), the initial transient conductivity at

Δt = 0 ps shows almost Drude-like free carrier response. At Δt = 0.5 ps, the response contains both Drude response and defect oscillators. Later when Δt = 1 ps, the contributions from the high-frequency oscillators associated with defect trapping are dominant. The decay process is concurrently illustrated in the inset of Figure 4, where the density of defects (T_i) is schematically shown as a width of square. γ_t and γ_{Auger} are the decay *via* defect trapping and Auger process, respectively.

These different THz responses between the annealed GO and the pristine GO sample can be understood by comparing the relative ratio between $\omega_p{}^2$ (Drude weight) and $\sum_{k=1}^{3} \omega_{L,\ k}{}^2$ (sum of oscillator weight). For the case of 600 °C annealed GO sample, the ratio of Drude weight ($[\omega_p/2\pi]^2$ = 7225 THz^2) to other oscillators ($\sum_{k=1}^{3} [\omega_{L,k}/2\pi]^2$ = 5013 THz^2) at Δt = 0 is 1.44: 1. Because the photoexcitation density (1.2×10^{12} cm^{-2}) is well above the defect density (0.8×10^{11} cm^{-2}), the decay through defect trapping is easily saturated. The third-order-power dependence in Figure 2b supports the THz data that the rapid carrier relaxation is indeed governed by the Auger recombination pathway. The increasingly large Auger coefficient obtained *via* rate-equation analyses further substantiates our observation. Thus, the coexistence of Drude and oscillator response can be understood by the effects of defect saturation (multiple oscillators) and free-carrier response. When Δt is 0.5 ps, the ratio of Drude weight to the other oscillators is reversed to 1:6.8. This can be understood by considering both the rapidly decreased DC conductivity (by Auger recombination) and the slowly appeared response of high frequency-oscillators by defect trapping. At Δt = 1 ps, because the free carrier responses are almost vanished, the remaining response can be explained by the oscillators alone. It is interesting to note that the above transient conductivity dynamics is similar to that of the all annealed GO samples, except the pristine GO sample. It means that the relaxation pathway of carrier dynamics is abruptly switched from the defect-dominated relaxation to the Auger recombination when the annealing temperature is increased above 200 °C.

CONCLUSIONS

In conclusion, we have investigated the kinetic origin of rapid carrier relaxation in a various set of GO samples. The pristine GO sample has a decay channel dominated by defect trapping with a monoexponential decay, which leads to a linear F dependence. When the annealing temperature increases higher than 200 °C, we have observed a new decay channel induced by Auger recombination. The threshold F was 50 μJ/cm^2, and the peak conductivity is proportional to the cubic square root of F. The coupled rate equation including defect trapping and Auger recombination explains well the time-resolved decay dynamics. Spectrally resolved transient THz conductivity strongly corroborates that the Auger recombination becomes dominant after saturating the defect states. We believe that these investigations will provide experimentally valuable insights in future studies to understand the carrier relaxation dynamics in GO or in developing ultrafast GO-based optoelectronic devices.

METHODS.

Preparation of Pristine and Annealed GO Samples. We prepared GO samples from graphite powder by modified Hummer's method.[54] First, the natural graphite powder was mixed with potassium peroxodisulfate and phosphorus pentoxide in sulfur acid condition and the solution was stirred at 80 °C for 10 min. The resultant mixture, then, was cooled down to room temperature and stirred for 6 h. Second, the mixture was rinsed with deionized water and filtered until it became neutral. After drying the preoxidated graphite overnight, dried graphite was oxidized again with potassium permanganate at 0 °C in ice bath until the graphite was totally oxidant with slow rate. Third, the product was aged and stirred at 35 °C for 2 h with distilled water. After the reaction was terminated, a large amount of water and hydro peroxide was added, followed by filtering and washing with HCl in order to eliminate metal ions from oxidants. Finally, after dialysis of oxidized graphite, the suspension was exfoliated by sonication and centrifuged to remove graphite powder not reacting with oxidant.

Conflict of Interest: The authors declare no competing financial interest.

Acknowledgment. J. Kim and H. Choi were supported by the National Research Foundation of Korea (NRF) grant funded by the Korea government (MSIP) (NRF-2011-0013255, NRF-2011-220-D00052, NRF-2011-0028594, NRF-2009-0083512, NRF-2012R1A1A2043180) and the LG Display Academic Industrial Cooperation Program. Y.-S. Lee was supported by the National Research Foundation of Korea (NRF) grant funded by the Korea government (MSIP) (NRF-2011-220-D00052). J. Oh and S. C. Jun were supported by the Priority Research Centers Program (2012-8-1663) and the Pioneer Research Center Program (2012-0000428) through the National Research Foundation of Korea (NRF) funded by the Ministry of Education, Science and Technology (MEST) of the Korean government.

Supporting Information Available: Bruggeman effective medium approximation, thin-film conductivity formula for the measured THz fields, and more detailed optical-pump THz-probe spectroscopy. This material is available free of charge *via* the Internet at http://pubs.acs.org.

Note Added after ASAP Publication: This paper was published ASAP on February 10, 2014, with an incorrect version of Supporting Information. Revised Supporting Information was reposted with the article on February 14, 2014.

REFERENCES AND NOTES

1. Novoselov, K. S.; Geim, A. K.; Morozov, S. V.; Jiang, D.; Katsnelson, M. I.; Grigorieva, I. V.; Dubonos, S. V.; Firsov, A. A. Two-Dimensional Gas of Massless Dirac Fermions in Graphene. *Nature* **2005**, *438*, 197–200.
2. Zhang, Y.; Tan, Y. W.; Stormer, H. L.; Kim, P. Experimental Observation of the Quantum Hall Effect and Berry's Phase in Graphene. *Nature* **2005**, *438*, 201–204.
3. Castro Neto, A. H.; Guinea, F.; Peres, N. M. R.; Novoselov, K. S.; Geim, A. K. The Electronic Properties of Graphene. *Rev. Mod. Phys.* **2009**, *81*, 109–162.

4. Kim, K. S.; Zhao, Y.; Jang, H.; Lee, S. Y.; Kim, J. M.; Kim, K. S.; Ahn, J. H.; Kim, P.; Choi, J. Y.; Hong, B. H. Large-Scale Pattern Growth of Graphene Films for Stretchable Transparent Electrodes. *Nature* **2009**, *457*, 706–710.
5. Gilje, S.; Han, S.; Wang, M.; Wang, K. L.; Kaner, R. B. A Chemical Route to Graphene for Device Applications. *Nano Lett.* **2007**, *7*, 3394–3398.
6. Gómez-Navarro, C.; Weitz, R. T.; Bittner, A. M.; Scolari, M.; Mews, A.; Burghard, M.; Kern, K. Electronic Transport Properties of Individual Chemically Reduced Graphene Oxide Sheets. *Nano Lett.* **2007**, *7*, 3499–3503.
7. Eda, G.; Fanchini, G.; Chhowalla, M. Large-Area Ultrathin Films of Reduced Graphene Oxide as a Transparent and Flexible Electronic Material. *Nat. Nanotechnol.* **2008**, *3*, 270–274.
8. Gao, W.; Alemany, L. B.; Ci, L.; Ajayan, P. M. New Insights into the Structure and Reduction of Graphite Oxide. *Nat. Chem.* **2009**, *1*, 403–408.
9. Bagri, A.; Mattevi, C.; Acik, M.; Chabal, Y. J.; Chhowalla, M.; Shenoy, V. B. Structural Evolution during the Reduction of Chemically Derived Graphene Oxide. *Nat. Chem.* **2010**, *2*, 581–587.
10. Zhu, Y.; Murali, S.; Cai, W.; Li, X.; Suk, J. W.; Potts, J. R.; Ruoff, R. S. Graphene and Graphene Oxide: Synthesis, Properties, and Applications. *Adv. Mater.* **2010**, *22*, 3906–3924.
11. Jeong, H. K.; Jin, M. H.; So, K. P.; Lim, S. C.; Lee, Y. H. Tailoring the Characteristics of Graphite Oxides by Different Oxidation Times. *J. Phys. D: Appl. Phys.* **2009**, *42*, 065418-1–065418-6.
12. Eda, G.; Mattevi, C.; Yamaguchi, H.; Kim, H.; Chhowalla, M. Insulator to Semimetal Transition in Graphene Oxide. *J. Phys. Chem. C* **2009**, *113*, 15768–15771.
13. Acik, M.; Lee, G.; Mattevi, C.; Chhowalla, M.; Cho, K.; Chabal, Y. J. Unusual Infrared-Absorption Mechanism in Thermally Reduced Graphene Oxide. *Nat. Mater.* **2010**, *9*, 840–845.
14. Loh, K. P.; Bao, Q.; Eda, G.; Chhowalla, M. Graphene Oxide as a Chemically Tunable Platform for Optical Applications. *Nat. Chem.* **2010**, *2*, 1015–1024.
15. Rani, J. R.; Lim, J.; Oh, J.; Kim, J. W.; Shin, H. S.; Kim, J. H.; Lee, S.; Jun, S. C. Epoxy to Carbonyl Group Conversion in Graphene Oxide Thin Films: Effect on Structural and Luminescent Characteristics. *J. Phys. Chem. C* **2012**, *116*, 19010–19017.
16. Dawlaty, J. M.; Shivaraman, S.; Chandrashekhar, M.; Rana, F.; Spencer, M. G. Measurement of Ultrafast Carrier Dynamics in Epitaxial Graphene. *Appl. Phys. Lett.* **2008**, *92*, 042116-1–042116-3.
17. Zou, X. Q.; Zhan, D.; Fan, X. F.; Lee, D.; Nair, S. K.; Sun, L.; Ni, Z. H.; Luo, Z. Q.; Liu, L.; Yu, T.; *et al.* Ultrafast Carrier Dynamics in Pristine and $FeCl_3$-Intercalated Bilayer Graphene. *Appl. Phys. Lett.* **2010**, *97*, 141910-1–141910-3.
18. Sun, D.; Wu, Z.-K.; Divin, C.; Li, X.; Berger, C.; de Heer, W. A.; First, P. N.; Norris, T. B. Ultrafast Relaxation of Excited Dirac Fermions in Epitaxial Graphene Using Optical Differential Transmission Spectroscopy. *Phys. Rev. Lett.* **2008**, *101*, 157402-1–157402-4.
19. Choi, H.; Borondics, F.; Siegel, D. A.; Zhou, S. Y.; Martin, M. C.; Lanzara, A.; Kaindl, R. A. Broadband Electromagnetic Response and Ultrafast Dynamics of Few-Layer Epitaxial Graphene. *Appl. Phys. Lett.* **2009**, *94*, 172102-1–172102-3.
20. Breusing, M.; Kuehn, S.; Winzer, T.; Malic, E.; Milde, F.; Severin, N.; Rabe, J. P.; Ropers, C.; Knorr, A.; Elsaesser, T. Ultrafast Nonequilibrium Carrier Dynamics in a Single Graphene Layer. *Phys. Rev. B* **2011**, *83*, 153410-1–153410-4.
21. Winnerl, S.; Orlita, M.; Plochocka, P.; Kossacki, P.; Potemski, M.; Winzer, T.; Malic, E.; Knorr, A.; Sprinkle, M.; Berger, C.; *et al.* Carrier Relaxation in Epitaxial Graphene Photoexcited Near the Dirac Point. *Phys. Rev. Lett.* **2011**, *107*, 237401-1–237401-5.
22. Li, T.; Luo, L.; Hupalo, M.; Zhang, J.; Tringides, M. C.; Schmalian, J.; Wang, J. Femtosecond Population Inversion and Stimulated Emission of Dense Dirac Fermions in Graphene. *Phys. Rev. Lett.* **2012**, *108*, 167401-1–167401-5.
23. Winzer, T.; Knorr, A.; Mittendorff, M.; Winnerl, S.; Lien, M. B.; Sun, D.; Norris, T. B.; Helm, M.; Malic, E. Absorption Saturation in Optically Excited Graphene. *Appl. Phys. Lett.* **2012**, *101*, 221115-1–221115-4.
24. Winzer, T.; Malic, E. The Impact of Pump Fluence on Carrier Relaxation Dynamics in Optically Excited Graphene. *J. Phys.: Condens. Matter.* **2013**, *25*, 054201-1–054201-7.
25. Wang, X.; Zhi, L.; Müllen, K. Transparent, Conductive Graphene Electrodes for Dye-Sensitized Solar Cells. *Nano Lett.* **2008**, *8*, 323–327.
26. Stoller, M. D.; Park, S.; Yanwu, Z.; An, J.; Ruoff, R. S. Graphene-Based Ultracapacitors. *Nano Lett.* **2008**, *8*, 3498–3502.
27. Gabor, N. M.; Song, J. C. W.; Ma, Q.; Nair, N. L.; Taychatanapat, T.; Watanabe, K.; Taniguchi, T.; Levitov, L. S.; Jarillo-Herrero, P. Hot Carrier-Assisted Intrinsic Photoresponse in Graphene. *Science* **2011**, *334*, 648–652.
28. Yan, J.; Kim, M. H.; Elle, J. A.; Sushkov, A. B.; Jenkins, G. S.; Milchberg, H. M.; Fuhrer, M. S.; Drew, H. D. Dual-Gated Bilayer Graphene Hot-Electron Bolometer. *Nat. Nanotechnol.* **2012**, *7*, 472–478.
29. Tans, S. J.; Verschueren, A. R. M.; Dekker, C. Room-Temperature Transistor Based on a Single Carbon Nanotube. *Nature* **1998**, *393*, 49–52.
30. Kong, J.; Franklin, N. R.; Zhou, C.; Chapline, M. G.; Peng, S.; Cho, K.; Dai, H. Nanotube Molecular Wires as Chemical Sensors. *Science* **2000**, *287*, 622–625.
31. Baughman, R. H.; Zakhidov, A. A.; De Heer, W. A. Carbon Nanotubes—The Route Toward Aplications. *Science* **2002**, *297*, 787–792.
32. O'Connell, M. J.; Bachilo, S. H.; Huffman, C. B.; Moore, V. C.; Strano, M. S.; Haroz, E. H.; Rialon, K. L.; Boul, P. J.; Noon, W. H.; Kittrell, C.; *et al.* Band Gap Fluorescence From Individual Single-Walled Carbon Nanotubes. *Science* **2002**, *297*, 593–596.
33. Murray, C. B.; Kagan, C. R.; Bawendi, M. G. Self-Organization of CdSe Nanocrystallites into Three-Dimensional Quantum Dot Superlattices. *Science* **1995**, *270*, 1335–1338.
34. Alivisatos, A. P. Semiconductor Clusters, Nanocrystals, and Quantum Dots. *Science* **1996**, *271*, 933–937.
35. Chan, W. C. W.; Nie, S. Quantum Dot Bioconjugates for Ultrasensitive Nonisotopic Detection. *Science* **1998**, *281*, 2016–2018.
36. Jung, G. B.; Myung, Y.; Cho, Y. J.; Sohn, Y. J.; Jang, D. M.; Kim, H. S.; Lee, C. W.; Park, J.; Maeng, I.; Son, J. H.; *et al.* Terahertz Spectroscopy of Nanocrystal-Carbon Nanotube and -Graphene Oxide Hybrid Nanostructures. *J. Phys. Chem. C* **2010**, *114*, 11258–11265.
37. Choi, K.; Lim, J.; Rani, J. R.; Yoon, H. S.; Oh, J.; Hong, T.; Ha, T.; Park, B. C.; Sim, K. I.; Jun, S. C.; *et al.* Terahertz and Optical Study of Monolayer Graphene Processed by Plasma Oxidation. *Appl. Phys. Lett.* **2013**, *102*, 131901-1–131901-4.
38. Ruzicka, B. A.; Werake, L. K.; Zhao, H.; Wang, S.; Loh, K. P. Femtosecond Pump-Probe Studies of Reduced Graphene Oxide Thin Films. *Appl. Phys. Lett.* **2010**, *96*, 173106-1–173106-3.
39. Zhao, X.; Liu, Z. B.; Yan, W. B.; Wu, Y.; Zhang, X. L.; Chen, Y.; Tian, J. G. Ultrafast Carrier Dynamics and Saturable Absorption of Solution-Processable Few-Layered Graphene Oxide. *Appl. Phys. Lett.* **2011**, *98*, 121905-1–121905-3.
40. Moulder, J. F.; Stickle, W. F.; Sobol, P. E.; Bomben, K. D. *Handbook of X-ray Photoelectron Spectroscopy*; Physical Electronics Inc.: Eden Prairie, MN, 1995.
41. Park, E. D.; Lee, J. S. Effects of Pretreatment Conditions on CO Oxidation over Supported Au Catalysts. *J. Catal.* **1999**, *186*, 1–11.
42. Yang, L.; Deslippe, J.; Park, C.-H.; Cohen, M. L.; Louie, S. G. Excitonic Effects on the Optical Response of Graphene and Bilayer Graphene. *Phys. Rev. Lett.* **2009**, *103*, 186802-1–186802-4.
43. Kim, J.; Lim, S. C.; Chae, S. J.; Maeng, I.; Choi, Y.; Cha, S.; Lee, Y. H.; Choi, H. Ultrafast Zero Balance of the Oscillator-Strength Sum Rule in Graphene. *Sci. Rep.* **2013**, *3*, 2663-1–2663-5.

44. Hong, J. T.; Lee, K. M.; Son, B. H.; Park, S. J.; Park, D. J.; Park, J. Y.; Lee, S.; Ahn, Y. H. Terahertz Conductivity of Reduced Graphene Oxide Films. *Opt. Express* **2013**, *21*, 7633–7640.
45. George, P. A.; Strait, J.; Dawlaty, J.; Shivaraman, S.; Chandrashekhar, M.; Rana, F.; Spencer, M. G. Ultrafast Optical-Pump Terahertz-Probe Spectroscopy of the Carrier Relaxation and Recombination Dynamics in Epitaxial Graphene. *Nano Lett.* **2008**, *8*, 4248–4251.
46. Jnawali, G.; Rao, Y.; Yan, H.; Heinz, T. F. Observation of a Transient Decrease in Terahertz Conductivity of Single-Layer Graphene Induced by Ultrafast Optical Excitation. *Nano Lett.* **2013**, *13*, 524–530.
47. Sosnowski, T. S.; Norris, T. B.; Wang, H. H.; Grenier, P.; Whitaker, J. F.; Sung, C. Y. High-Carrier-Density Electron Dynamics in Low-Temperature-Grown GaAs. *Appl. Phys. Lett.* **1997**, *70*, 3245–3247.
48. Ghosh, S.; Bhattacharya, P.; Stoner, E.; Singh, J.; Jiang, H.; Nuttinck, S.; Laskar, J. Temperature-Dependent Measurement of Auger Recombination in Self-Organized $In_{0.4}Ga_{0.6}As$/GaAs Quantum Dots. *Appl. Phys. Lett.* **2001**, *79*, 722–724.
49. Ortiz, V.; Nagle, J.; Lampin, J. F.; Peronne, E.; Alexandrou, A. Low-Temperature-Grown GaAs: Modeling of Transient Reflectivity Experiments. *J. Appl. Phys.* **2007**, *102*, 043515-1–043515-9.
50. Jepsen, P. U.; Schairer, W.; Libon, I. H.; Lemmer, U.; Hecker, N. E.; Birkholz, M.; Lips, K.; Schall, M. Ultrafast Carrier Trapping in Microcrystalline Silicon Observed in Optical Pump-Terahertz Probe Measurements. *Appl. Phys. Lett.* **2001**, *79*, 1291–1293.
51. Parkinson, P.; Joyce, H. J.; Gao, Q.; Tan, H. H.; Zhang, X.; Zou, J.; Jagadish, C.; Herz, L. M.; Johnston, M. B. Carrier Lifetime and Mobility Enhancement in Nearly Defect-Free Core-Shell Nanowires Measured Using Time-Resolved Terahertz Spectroscopy. *Nano Lett.* **2009**, *9*, 3349–3353.
52. Bruggeman, D. A. G. Berechnung Verschiedener Physikalischer Konstanten Von Heterogenen Substanzen. I. Dielektrizitätskonstanten und Leitfähigkeiten der Mischkörper aus Isotropen Substanzen. *Ann. Phys.* **1935**, *416*, 636–664.
53. Tsai, Y.-J.; Chang, C.-Y.; Lai, Y.-C.; Yu, P.-C.; Ahn, H. Realization of Metal−Insulator Transition and Oxidation in Silver Nanowire Percolating Networks by Terahertz Reflection Spectroscopy. *ACS Appl. Mater. Interfaces* **2013**, *6*, 630–635.
54. Hummers, W. S.; Offeman, R. E. Preparation of Graphitic Oxide. *J. Am. Chem. Soc.* **1958**, *80*, 1339–1339.